Thermodynamics of biexcitons in a GaAs quantum well

J. C. Kim, D. R. Wake, and J. P. Wolfe
Physics Department and Frederick Seitz Materials Research Laboratory, University of Illinois at Urbana-Champaign, Urbana, Illinois 61801
(Received 31 May 1994)

Photoluminescence from GaAs quantum wells displays sharp spectral features associated with the free exciton. At high excitation density and low temperature, an additional component appears just below the lowest (heavy-hole) excitonic emission. Previous studies have attributed this feature to the biexciton, consisting of two electrons and two holes, because it appears below the exciton line and grows superlinearly with respect to the exciton intensity. In this paper, we considerably strengthen this identification by analyzing time- and space-resolved photoluminescence data that imply a dynamic chemical equilibrium between the excitons and biexcitons, i.e., a law of mass action. This thermodynamic (complementary to spectroscopic) evidence for biexcitons is based on the interdependent temporal decay and spatial transport behavior of the two components on a picosecond time scale. As the excitons recombine, the law of mass action describes the equilibrium over more than two orders of magnitude in exciton density as determined from the measured photoluminescence intensity and volume of the exciton gas.

I. INTRODUCTION

The free exciton, or an electron and a hole bound by Coulomb attraction, is a fundamental excited state of a semiconductor. Absorption and photoluminescence spectra of most semiconductors at low temperature show sharp features associated with this state. The free exciton (or simply "exciton") is a mobile particle capable of diffusing through the crystal, interacting with other excitons, and possibly becoming trapped at impurity sites, before the constituent electron-hole pair recombines. The exciton can display properties similar to an atomic gas, such as combining into excitonic molecules, condensing into an electron-hole liquid, or exhibiting coexistence of two or more of these phases in equilibrium. These manifestations of "chemical equilibrium" are generally displayed in the indirect-gap semiconductors such as Ge and Si whose carrier lifetimes are on the order of microseconds.[1]

The simplest excitonic molecule is a biexciton comprised of two electrons and two holes, analogous to a hydrogen molecule. Whereas in bulk indirect-gap semiconductors biexcitons have been conclusively observed,[1,2] in a bulk crystal of the direct-gap semiconductor GaAs, observation of this simplest molecular species is difficult. This is because in GaAs the exciton lifetime is typically about a nanosecond, limiting the exciton's diffusion length and its ability to thermalize to the lattice temperature. Further, the relatively small binding energy of the exciton in a bulk crystal of GaAs (4 meV) leads to a theoretical biexciton binding energy of only a few tenths of a meV. Consequently, the evidence so far for the existence of biexcitons in bulk GaAs is weak. However, within a GaAs quantum well of thickness less than 100 Å which is less than the 150-Å excitonic Bohr radius in bulk GaAs, the confinement doubles the exciton binding energy[3] to about 8 meV. In this case, the predicted biexciton binding energy[4] is larger than 1 meV, and indeed, Miller *et al.*[5] as well as others[6–8] have reported evidence for the biexcitons in GaAs multiple quantum wells (MQW's) from their photoluminescence data. Their data show a spectral peak below the heavy-hole excitonic emission, whose intensity increases superlinearly with excitation density.

In this paper, we examine the character of this spectral feature from a thermodynamic perspective. We use time-resolved photoluminescence spectroscopy and spatial imaging to observe the relative densities of the excitonic species for several lifetimes after a short laser pulse.[9] The data imply a law of mass action consistent with a thermodynamic and chemical equilibrium between the excitons and biexcitons in a GaAs MQW, strongly supporting the biexciton identification. An important aspect of this work is the measurement of the spatial profiles of the two excitonic components, from which we obtain an effective "volume" of each, actually an effective "area" occupied by each gas in the narrow quantum well. The area measurements are necessary for ascertaining the relative areal densities of the excitons and biexcitons. The ratio of the areas of the two species agrees with the prediction based on the law of mass action, adding support to the self-consistency of our analysis and interpretation of the data.

II. CHEMICAL KINETICS OF EXCITONS AND BIEXCITONS

Excitons produced by photoexcitation are inherently a nonequilibrium species because the energy gap E_{GAP} separating the conduction band from the valence band is much greater than $k_B T_L$ where T_L is the lattice temperature. As the electron-hole pairs recombine, the decaying excitons emit photons and/or phonons. In undoped GaAs, the photoluminescence from radiatively recombin-

ing *free* excitons contains no direct information about the kinetic-energy distribution of the particles because only the excitons near zone center having momentum $\mathbf{k} \approx \mathbf{k}_{\text{PHOTON}}$ and energy $E_X = E_{\text{GAP}} - \phi_X$ can radiatively recombine, where $\mathbf{k}_{\text{PHOTON}}$ is the momentum of the emitted photon and ϕ_X is the binding energy of an exciton with respect to an ionized electron-hole pair. If the kinetic-energy distribution of the excitons is described by a Maxwell-Boltzmann distribution with an effective temperature T_E, and the optical transition has a homogeneous linewidth $\Gamma \ll k_B T_E$, the measured luminescence intensity from N_X excitons is

$$I_X = C \left[\frac{N_X}{\tau_r} \right] \left[\frac{\Gamma}{k_B T_E} \right] , \tag{1}$$

where the constant C includes the optical collection efficiency and τ_r is the radiative lifetime for an exciton with $\mathbf{k} \approx \mathbf{k}_{\text{PHOTON}}$.[10] It is useful to think of the effective radiative lifetime of the excitons as τ_r divided by $\Gamma/(k_B T_E)$ which is the fraction of excitons near $\mathbf{k} \approx \mathbf{k}_{\text{PHOTON}}$ capable of radiative recombination.

The time required for excitons to achieve a Maxwellian distribution after a short generation pulse depends on the initial exciton density. For the densities studied in this paper, interparticle collisions occur on a subpicosecond time scale, so to a good approximation the exciton gas (including excitons and biexcitons) has an internal *thermal* equilibrium characterized by T_E. On the other hand, since the excitons are created with nonzero kinetic energies and must relax by emitting acoustic-phonons, the time scale on which $T_E(t)$ approaches T_L is dictated by the exciton acoustic-phonon interaction time which may extend to several hundred picoseconds.

The *chemical* equilibrium between excitons and biexcitons in Si has been described in detail by Gourley and Wolfe.[2] For a given T_E, they consider a chemical equilibrium that implies a "law of mass action,"

$$\frac{n_X^2}{n_{XX}} = n^*(T_E) , \tag{2}$$

where n_X and n_{XX} are the exciton and biexciton densities. The equilibrium constant $n^*(T_E)$ is a "characteristic density" which has the form

$$n^*(T_E) = g n_Q \exp \left[\frac{-\phi_{XX}}{k_B T_E} \right] , \tag{3}$$

where g is the effective degeneracy factor, ϕ_{XX} is the binding energy of the biexciton with respect to two unbound excitons, and n_Q is the effective quantum concentration. For a three-dimensional gas of excitons and biexcitons with density-of-states masses m_X and m_{XX}

$$n_Q = \left[\frac{1}{2\pi\hbar^2} \frac{m_X^2}{m_{XX}} \right]^{3/2} (k_B T_E)^{3/2} . \tag{4}$$

For a two-dimensional gas inside a quantum well

$$n_Q = \left[\frac{1}{2\pi\hbar^2} \frac{m_X^2}{m_{XX}} \right] (k_B T_E) , \tag{5}$$

where, in this case, n_Q is an areal density.

In a practical experiment, one typically measures the total photoluminescence intensity which is proportional to the total number of excitons or biexcitons [see Eq. (1)]. However, one would like to measure the local densities of the gases because the thermodynamic expressions relate the local densities, not the total numbers. In the measurements on bulk Si,[2] the volume of the exciton gas was accurately controlled by confining the excitons in a three-dimensional parabolic strain well. Under confinement, the gas volume depends only on the gas temperature. Due to the long recombination times in Si, the gas temperature was equal to the lattice temperature during the measurement. Consequently, the gas volume remained constant during the measurement, and the photoluminescence intensity accurately indicated the density.

In a quantum well, although the particles are confined in the direction normal to the well plane, lateral diffusion allows the effective area occupied by the gas to increase in time. We show later in this paper that, under specified conditions, the distribution of the excitons in the plane of a 100-Å quantum well takes on a Gaussian form. So, for the exciton component, the spatially averaged areal density $\bar{n}_X$ is related to the total intensity by $\bar{n}_X \propto I_X/\Delta_X^2$, where Δ_X is the full width at half maximum (FWHM) of the Gaussian. Δ_X^2 is the effective area occupied by the exciton gas, and because Δ_X^2 increases during measurement due to diffusion, $\bar{n}_X$ is not simply proportional to I_X. Fortunately, $\bar{n}_X$ can be obtained by combining time-resolved measurements of the total luminescence intensity (proportional to the total number) and the effective area.

The equilibrium constant n^* [see Eq. (3)] depends on the biexciton binding energy which depends on the well width. In Fig. 1, we plot the theoretical biexciton binding energies obtained from Ref. 4 for several well widths.

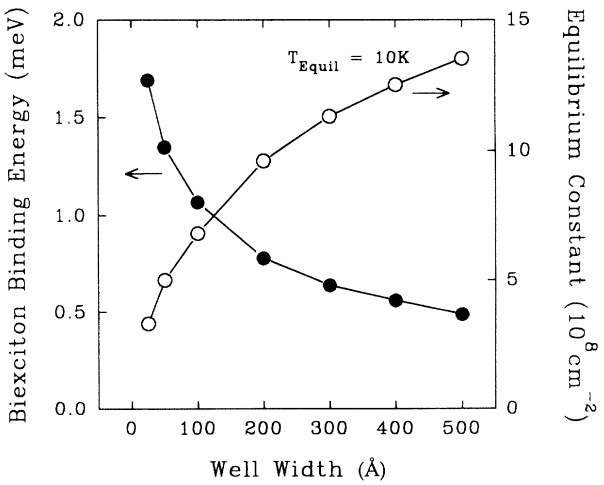

FIG. 1. Solid circles show biexciton energies for various well widths obtained from Ref. 4, and open circles show corresponding equilibrium constants [given by Eqs. (3)] at an equilibrium temperature of 10 K. Solid lines serve as guides to the eye. As the well width decreases, the biexciton binding energy increases, and the biexciton concentration significantly increases relative to the free exciton concentration.

To see how the confinement in a quantum well affects chemical equilibrium, we also plot n^* for an equilibrium temperature of 10 K for the same well widths in Fig. 1. The increased binding energy due to confinement is predicted to significantly increase the relative biexciton density at a given exciton density through n^*.

III. EXPERIMENTAL METHODS

A schematic of our time-resolved photoluminescence-imaging apparatus is presented in Fig. 2. As shown in Fig. 2(a) we excite a 10-period, 100-Å GaAs MQW with a 5-ps laser pulse at 76 MHz. Both the laser beam and the detector field of view can be tightly focused to 3-μm spots on the sample inside an optical cryostat, yielding a resultant spatial resolution of 4 μm. The excitation energy is tuned to the light-hole exciton absorption peak where enhanced photoabsorption and fast interconversion between light-hole excitons and heavy-hole excitons result in efficient generation of the heavy-hole excitons. Within the excitation spot, an average power of 1 mW corresponds to each pulse creating a nominal pair density of 10^{12} cm^{-2} carriers within each well, although the actual densities may be lower by a factor of 2 or 3. As shown in Fig. 2(b) the luminescence from the radiatively recombining excitons is dispersed by a half-meter spectrometer and detected by a Hamamatsu micro-channel-plate detector in photon-counting mode. Conventional electronic techniques are employed to generate time traces of the photoluminescence decays[11] with temporal resolution of 36 ps.

We obtain time-resolved energy spectra by recording time traces as the detection (spectrometer) wavelength is incremented. The series of time traces are stored as a two-dimensional array which, when sliced at a particular time, yields a "snap shot" of the photoluminescence at that time. Likewise, by collecting time traces at a fixed detection wavelength while scanning the excitation spot

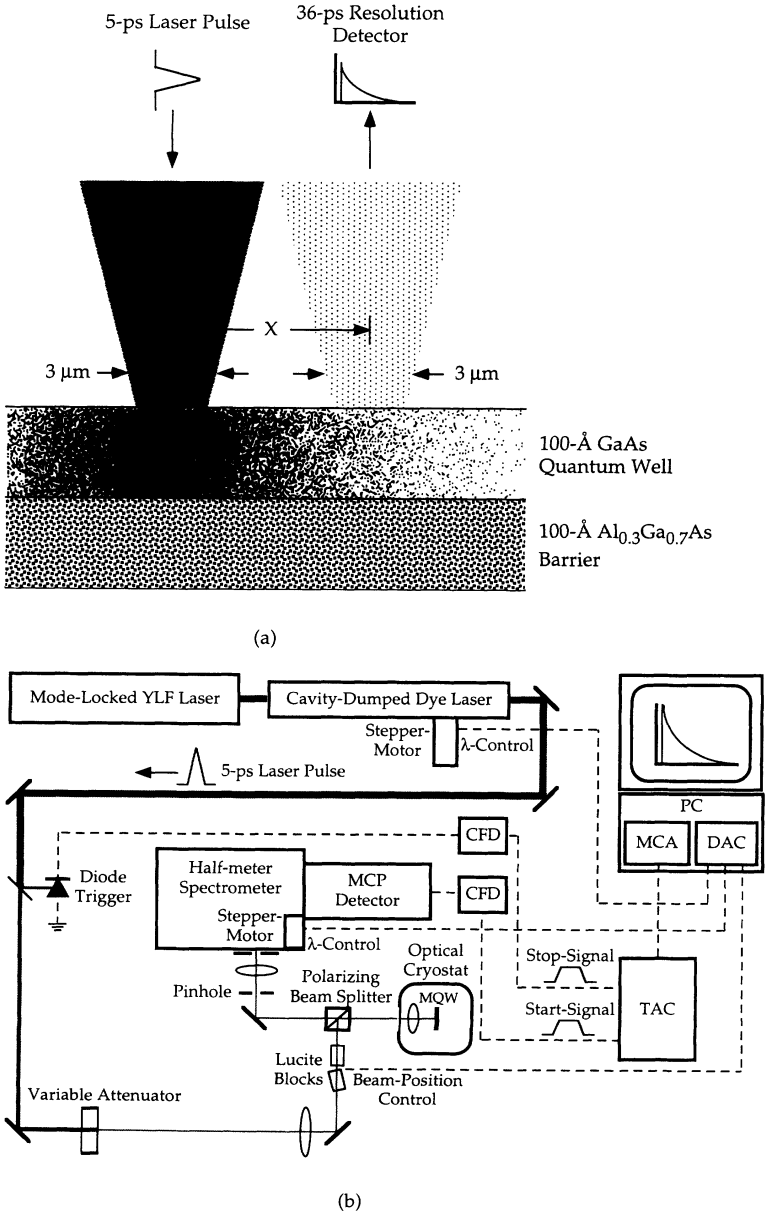

FIG. 2. (a) A schematic side view of the excitation area on the MQW sample. The detector field of view and the excitation spot can be moved (i.e., X changed in the figure) relative to each other for imaging. Inside the well, the strength of the shade indicates electron-hole pair density. (b) Time-correlated-photon-counting (TCPC) apparatus to measure time- and space-resolved photoluminescence. For more detail on the TCPC technique see Ref. 11.

about the detection spot in the plane of the MQW, we obtain time-resolved images of the excitation area. A snapshot of the spatial profile at a particular time is obtained by slicing the collection at that particular time.

The heavy-hole exciton peak in our sample has a 0.9-meV absorption width. The luminescence peak is Stokes shifted 0.3 meV from the absorption peak. The small Stokes shift suggests that interface islands significantly larger than the Bohr radius of the exciton are not prevalent. On the other hand, our analysis below implies an extremely small measured diffusivity, 14 $cm^2 sec^{-1}$, which suggest that well-width fluctuations comparable to or smaller than the excitonic Bohr radius are likely. A second MQW structure with 78 periods of an 80-Å GaAs well and a 100-Å Al_xGa_{1-x} GaAs barrier has yielded results that agree with the results reported for the 100-Å MQW.

IV. ANALYSIS OF RESULTS

A. Time-integrated spectra

Time-integrated spectra of the 100-Å MQW at $T_L = 10$ K are shown in Fig. 3(a) for pump power spanning 0.003–3 mW corresponding to initial pair densities 3×10^9–3×10^{12} cm^{-2}. To compare the line shapes, the spectra are normalized to the peak exciton intensity at 1.543 eV. Below an initial pair density of 1×10^{10} cm^{-2}, the spectra show only the density-independent heavy-hole exciton line whose low-energy tail is attributed to imperfections in the confining potential of the quantum well. With more intense excitation, a peak at about 1.8 meV below the exciton peak grows superlinearly with respect to excitation density. This superlinear growth is not consistent with impurity or defect luminescence, which would saturate at high excitation density. On the other hand, it is consistent with biexcitons whose density is predicted to grow quadratically with respect to the exciton density. Although a superlinear growth might originate from an Auger-type process in which two nearby excitons simultaneously emit a photon and leave an ionized electron-hole pair, for such a process the luminescence peak would occur at $E_X - \phi_X$ where $\phi_X \approx 8$ meV for a 100-Å MQW (Ref. 3) which is significantly larger than 1.8 meV. The 1.8-meV separation between the peaks is close to the 1.5-meV separation for a 102-Å GaAs MQW reported by Lovering and co-workers,[7] but it is larger than the 1.1-meV binding energy predicted by Kleinman[4] by about 0.7 meV. The actual biexciton binding energy could, however, be smaller than 1.8 meV by as much as 0.3 meV due to the Stokes shift between excitonic absorption and photoluminescence.

For quantitative analyses it is necessary to spectrally deconvolve the exciton and biexciton components in the photoluminescence spectra. A complication is the low-energy tail associated with the exciton luminescence. To overcome it, the exciton line shape is empirically determined from a spectrum for a low pair density and scaled as the exciton component in a spectrum for a high pair density. The biexciton component is then fit to a Lorentzian line shape while the strength of the exciton line shape is adjusted, as illustrated in Fig. 3(b).

The biexciton luminescence arises from the radiative recombination of one of its two electron-hole pairs, leaving behind a daughter exciton. In this process the decaying biexciton need not have $\mathbf{k}=\mathbf{k}_{PHOTON}$ because the daughter exciton can absorb the necessary momentum to conserve energy and momentum. For a biexciton with kinetic energy equal to E, momentum conservation implies that the daughter exciton has $2E$. The energy of the emitted photon is, therefore, $E_X - \phi_{XX} - E$. Assuming that the biexciton kinetic energies are distributed according to a Maxwell-Boltzmann (MB) distribution, this reasoning suggests that the biexciton luminescence should be a mirror image of the asymmetric MB line shape because of the minus sign in front of E.

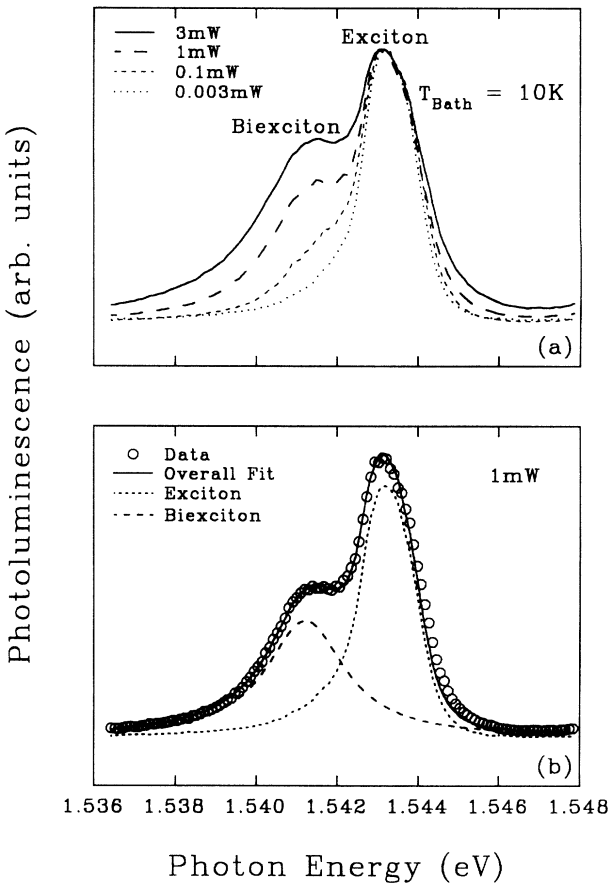

FIG. 3. (a) Time-integrated photoluminescence spectra at a bath temperature of 10 K for pump powers spanning 0.003–3 mW corresponding to initial pair densities 3×10^9–3×10^{12} cm^{-2}. To compare the line shapes the spectra are normalized to the peak height of the heavy-hole exciton luminescence at 1.543 eV. As the pump power (or initial pair density) is increased, the low-energy peak grows superlinearly with respect to the heavy-hole exciton peak. This growth behavior is consistent with a biexciton origin. (b) Deconvolution procedure to separate the exciton and biexciton components. The exciton line shape is empirically determined from a low-density spectrum and scaled as the exciton component in a high-density spectrum (pump power of 1 mW shown). The biexciton component is fit to a Lorentzian line shape.

Cho has shown, however, that for radiative recombination of one of the electron-hole pairs in a biexciton the momentum of the daughter exciton must be within about $|\mathbf{k}_0| = 1/a_{XX}$ of zero where a_{XX} is the Bohr radius of the biexciton.[12] This means that the momentum of the decaying biexciton must also be within about $|\mathbf{k}_0|$ of zero which implies that the kinetic energy of the biexciton does not exceed about $E_0 = \hbar^2/(2M_{XX}a_{XX}^2)$. For a 100-Å GaAs quantum well, $E_0 \approx 0.015$ meV using $a_{XX} \approx 1000$ Å as calculated by Kleinman.[4] Cho has shown that for $E_0/(k_B T_E) \approx 1.4$ the line shape resembles a symmetric Lorentzian and that the zero in biexciton kinetic energy (i.e., the band bottom) is nearly coincident with the peak of the line shape.[12] For $T_E \approx 10$ K in our experiments, $E_0/(k_B T_E) \ll 1.4$ so that a symmetric Lorentzian is an even better approximation to the biexciton line shape, with the peak of the line corresponding to emission from the biexcitonic band bottom. Indeed, empirically the symmetric Lorentzian line shape more accurately describes the biexciton component of the spectra than does the asymmetric MB line shape, as shown in Fig. 3(b).

The spectral weights (spectrally integrated intensities) of the deconvolved exciton and biexciton components [as in Fig. 3(b)] are plotted as functions of the pump power in Fig. 4. The data represent *time-integrated* spectra so each pair of data points (I_X, I_{XX}) at a given power corresponds to a time-averaged density and area occupied by the gas. Applying a straightforward kinetic theory to the data, the rate equations that describe the interconverting exciton-biexciton gas system under *continuous* generation[2] are

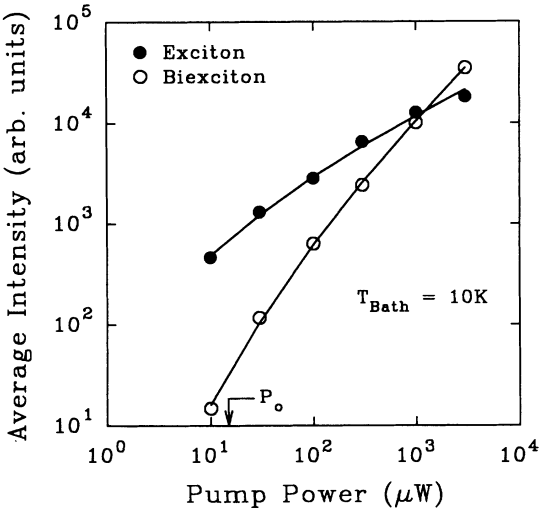

FIG. 4. Time-integrated exciton and biexciton spectral weights at a bath temperature of 10 K as functions of pump power. The solid lines are the steady-state solutions to a pair of rate equations that describe the interacting exciton-biexciton gas under continuous generation. The characteristic power P_0 is obtained from the fit and is proportional to the characteristic generation rate G_0 discussed in the text. The close agreement indicates that interconversion is much faster than decay.

$$\frac{dn_X}{dt} = G - \frac{n_X}{\tau_X} + \frac{n_{XX}}{\tau_{XX}} - 2\frac{n_X^2}{n^*}\frac{1}{\tau_C} + 2\frac{n_{XX}}{\tau_C}, \tag{6a}$$

$$\frac{dn_{XX}}{dt} = -\frac{n_{XX}}{\tau_{XX}} + \frac{n_X^2}{n^*}\frac{1}{\tau_C} - \frac{n_{XX}}{\tau_C}, \tag{6b}$$

where G is the continuous-generation rate (proportional to pump power), τ_X and τ_{XX} are the exciton and biexciton lifetimes, and τ_C is the characteristic interconversion time when $n_X = n_{XX} = n^*$. The two equations describe the generation of the excitons, the decays of the excitons and biexcitons, and the interconversion between them. The steady-state solutions to this pair of equations are

$$n_X \propto \left[\left[1+\frac{G}{G_0}\right]^{1/2} - 1\right], \tag{7a}$$

$$n_{XX} \propto \left[\left[1+\frac{G}{G_0}\right]^{1/2} - 1\right]^2, \tag{7b}$$

where $G_0 = (n^*\tau_{XX}/4\tau_X^2)(1+\tau_C/\tau_X)$ is the characteristic generation rate that separates the exciton-dominant from the biexciton-dominant region.[2] These equations predict that for low generation rates ($< G_0$) the dominant exciton population grows linearly and the biexciton population grows quadratically, while for high generation rates ($> G_0$) the dominant biexciton population grows linearly and the exciton population grows as the square root of the excitation, consistent throughout with $n_{XX} \propto n_X^2$. If the interconversion time is much faster than the recombination times and the observation time [i.e., the last two terms of Eq. (6a) dominate so that $n_{XX} \propto n_X^2$] then Eqs. (7) also apply to the initial densities produced by a short-pulsed excitation. In that case, $G \cong G_{\text{PULSE}}(\tau_{\text{PULSE}}/\tau_0)$ whereas G_{PULSE} is the average generation rate during the pulse, τ_{PULSE} is the duration of the pulse, and τ_0 is a characteristic lifetime of the excitonic gas. In Fig. 4, we plot n_X and n_{XX} in Eqs. (7) as the solid lines, with a single overall scaling factor and the characteristic power $P_0 = G_0 h\nu_{\text{LASER}} \times$ (excitation area) determined by the fit to the data. The close agreement between the data and the model in Fig. 4 implies that the interconversion time is indeed much shorter than the recombination times and the observation time, and that, consequently, thermal and chemical equilibrium is quickly established between the excitons and biexcitons in our MQW. However, a time-integrated spectrum represents an average of transient behavior, weighted by the instantaneous photon-emission rate. At best, this averaging may obscure important dynamic behavior, and at worst the good agreement between data and theory may be fortuitous. Thus, it is necessary to analyze the transient spectra to confidently assess the system behavior under pulsed-excitation conditions.

B. Time-resolved spectra

The relative populations of the excitons and biexcitons at a particular time are indicated by their spectral weights at that time. The spectral weights of the excitons and biexcitons are shown in Fig. 5(a) as functions of time

for an initial pair density of 10^{12} cm^{-2}. Each data point represents a particular time after the 5-ps laser pulse, from about 100 to 4000 ps. The plots reveal that the biexcitons decay twice as fast at the excitons, i.e., if $I_X \propto \exp(-t/\tau)$ then $I_{XX} \propto \exp(-2t/\tau)$, which implies $I_{XX}(t) \propto I_X^2(t)$. This display of thermodynamic and chemical equilibrium is consistent with an interconversion time that is much faster than the recombination times.

In Fig. 5(b) we take the data sets in Fig. 5(a) and plot them in a more illustrative form. We plot the spectral weight of the biexciton component, I_{XX}, as a function of the spectral weight of the exciton component, I_X, with time as the parametric variable. An additional data set corresponding to 10^{11}-cm^{-2} initial pair density is also plotted for a comparison. The upper-right corresponds to 100 ps and the lower left corresponds to 4000 ps. Two straight lines, each with a slope of 2 (square-law line), demonstrate that over a wide range in intensity the square-law of Eq. (2) describes each data set well. However, there are two notable discrepancies. First, there is a "hook" in the high-density data that suggests a relative deficiency of the exciton population at times up to about 500 ps. Second, the two data sets do not fall on the same square-law line, which implies different n^* for the two data sets even though n^* should depend only on temperature [see Eqs. (3)–(5)]. As we will see next, both of these anomalies can be traced to the fact that luminescence *intensity* is plotted in Fig. 5(b) rather than particle density. A given square-law line on a I_{XX} vs I_X plot is characterized by a fixed gas area, and if the area is different in the two runs, or changes during the carrier lifetime, the luminescence intensity will not consistently represent the areal density of the excitons or biexcitons.

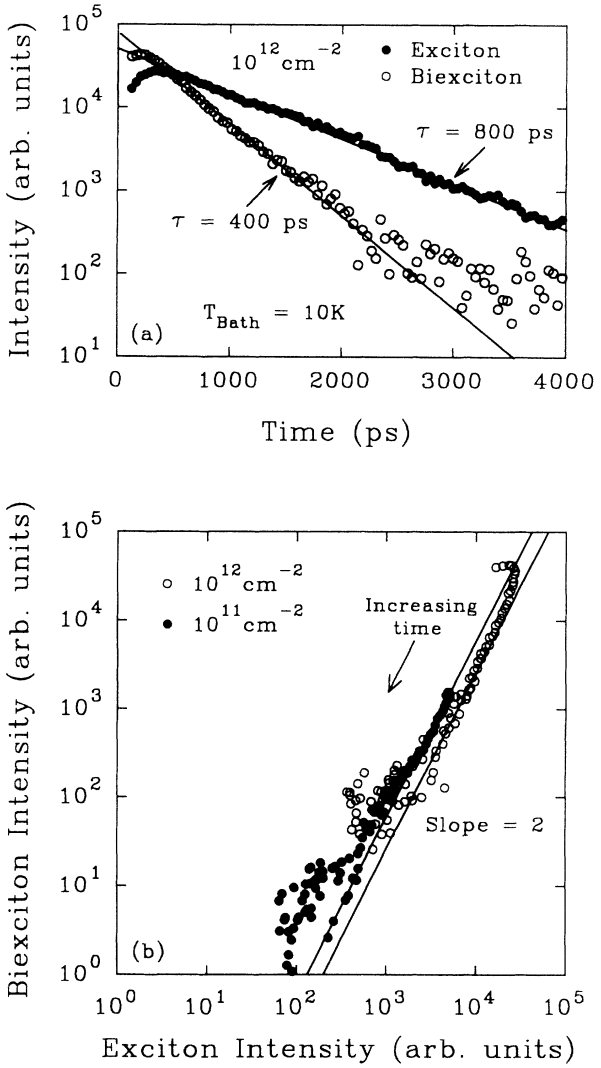

FIG. 5. (a) Spectral weights (spectrally integrated intensities) for excitons and biexcitons as functions of time for an initial pair density of 10^{12} cm^{-2} at a bath temperature of 10 K. The ratio of the decay constants is consistent with a chemical equilibrium described by a law of mass action and implies a fast interconversion. (b) The data sets in Fig. 5(a) are plotted against each other with time as the parametric variable. Another data set for an initial pair density of 10^{11} cm^{-2} is also plotted for a comparison. The square-law line describes chemical equilibrium for a gas occupying a fixed area. The two data sets corresponding to different initial pair densities do not fall on the same square-law line, implying that the gas areas for the different initial pair densities are not the same.

In our investigation, we have measured the instantaneous area occupied by the gas in the quantum well Δ^2 in addition to the instantaneous luminescence intensity (spectral weight), and from the two measurements we obtain the spatially averaged density, $\bar{n} \propto I/\Delta^2$. The detection wavelength is fixed at the peak of the excitonic (or biexcitonic) emission, and the time-dependent luminescence is obtained as a function of the position in the plane of the quantum well. The measured spatial profile of the gas defines the area occupied by the gas, as shown by the two-dimensional images in Figs. 6(a) and 6(b). Although the determination of the profile is complicated by the spectral overlap of the two excitonic components, the errors are small and do not modify the overall results if the strengths of the two components are comparable, i.e., at moderate to high pair densities.

The expansion behavior of the exciton gas in our system is apparent in Figs. 6(a) and 6(b). Within about 0.1 ns following the laser excitation pulse, the FWHM of the exciton profile shown in Fig. 6(a) is roughly equal to the FWHM of the excitation spot. After about 2.5 ns, the peak height has decreased while the FWHM has increased, as shown in Fig. 6(b). From the figures, it is clear that the exciton spatial profile is radially symmetric. A slice through the center of the exciton distribution for an initial pair density of 10^{12} cm^{-2} at $t \approx 700$ ps is plotted as the solid circles in Fig. 7(a). The Gaussian function,

$$n_X(r) = n_X(0) \exp\left[-\frac{r^2 \ln 16}{\Delta_X^2}\right], \tag{8a}$$

where Δ_X is the FWHM, describes this profile well as shown by the solid line through the solid circles. The biexciton spatial profile is shown by the open circles in Fig. 7(a) and is likewise well represented by a Gaussian,

but its FWHM is narrower than the exciton profile. In chemical equilibrium, because $n_{XX}(r) \propto n_X^2(r)$ everywhere in space, the biexciton density is predicted to follow the square of Eq. (8a), or

$$n_{XX}(r)=n_{XX}(0)\exp\left[-\frac{r^2 \ln 16}{\Delta_X^2/2}\right], \tag{8b}$$

and Δ_{XX}, the FWHM of the biexciton distribution, is related to Δ_X by $\Delta_X/\Delta_{XX}=\sqrt{2}$. From the data in Fig. 7(a), we find $\Delta_X/\Delta_{XX}=1.26$, which is not precisely equal to $\sqrt{2}$ as expected for local chemical equilibrium. However, the profiles in Fig. 7(a) are broadened by the instrumental resolution of about 4 μm. If we deconvolve from the exciton profile a Gaussian with 4-μm FWHM, the resulting Gaussian has $\Delta_X=\sqrt{\Delta^2_{X,\text{measured}}-16\ \mu\text{m}^2}$ and likewise for the biexciton profile. Figure 7(b) shows the deconvolved Gaussian functions for the two species from which we obtain $\Delta_X/\Delta_{XX}=1.43\pm0.09$, in good agreement with $\sqrt{2}$.

Figure 8(a) is a plot of the spatially deconvolved Δ_X^2 and Δ_{XX}^2 as functions of time after the 5-ps laser pulse. After about 500 ps the two gas areas continue to expand with $\Delta_{XX}^2/\Delta_X^2 \cong 0.5$, as expected for chemical equilibrium. The slope of the expansion line implies a diffusion constant $D=14$ cm^2 sec^{-1}, calculated using $D=(d\Delta_X^2/dt)/(16\ln 2)$, where the numerical factors come from the solution to the diffusion equation.[13] Figure 8(b) shows the ratios of the data points in Fig. 8(a) which, over the same time interval, cluster about the value 0.5, as expected. These space- and time-resolved photoluminescence measurements strongly indicate that chemical equilibrium is maintained during the diffusive expansion. In the first few hundred ps the expansion is more rapid and the excitons and biexcitons may be further away from equilibrium. Possible reasons for this are discussed later.

As previously indicated, the spatially averaged areal density of the excitons $\bar{n}_X(t)$ is simply proportional to

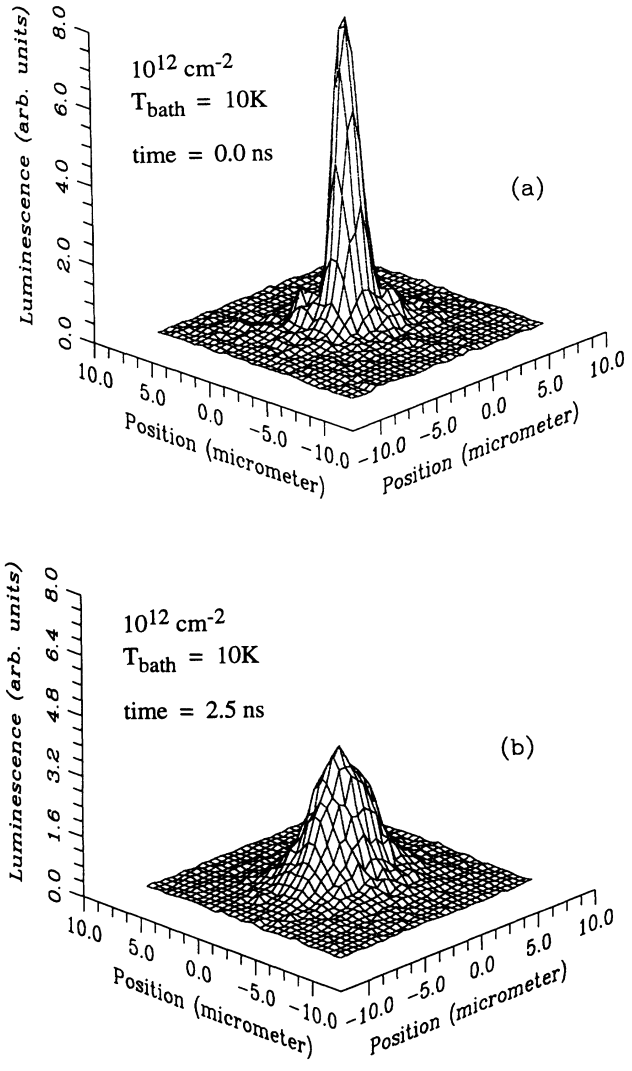

FIG. 6. (a) A pseudo-three-dimensional image of the spatial distribution of the excitons within about 100 ps following a pulsed laser excitation. The FWHM of the distribution is nearly equal to that of the excitation spot. (b) After about 2.5 ns the profile reveals a reduced peak and a broader distribution implying that the excitons have not only decayed but also diffused laterally from the initial excitation region.

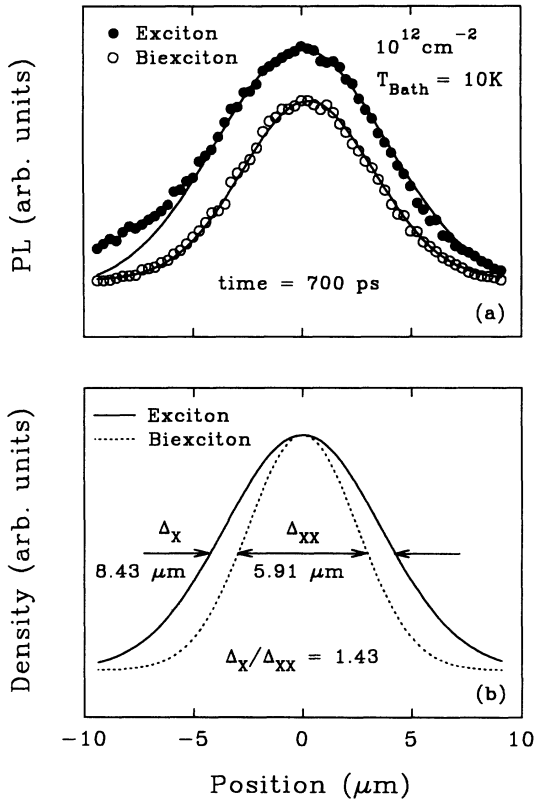

FIG. 7. (a) A slice through an image such as shown in Fig. 6(a) or 6(b) reveals a spatial distribution of excitons well described by a Gaussian function. Similarly, the biexciton distribution is well represented by a Gaussian with a smaller full width. (b) The Gaussian functions in Fig. 7(a) are deconvolved with a Gaussian function representing the instrumental resolution. The ratio of the deconvolved full widths is consistent with local chemical equilibrium.

$I_X(t)/\Delta_X^2(t)$, and similarly for the biexcitons. Figure 9(a) shows $\bar{n}_{XX}(t)$ vs $\bar{n}_X(t)$ for an initial pair density of 10^{12} cm^{-2}. The square-law line through the data points indicates that the excitons and biexcitons are in chemical equilibrium over more than two orders of magnitude in biexciton density. The hook feature in Fig. 5(b) is now absent because the expanding area has been taken into account. Evidently, fast interconversion allows the two species to quickly reach a well-defined thermal and chemical equilibrium. Figure 9(b) shows a similar plot for an initial pair density of 10^{11} cm^{-2}. Because the expansion is slow at low pair density, for this initial pair density the area correction does little to change the shape of the curve from that of Fig. 5(b); however, now the data for the two initial densities fall on the same square-law line to within experimental uncertainty.

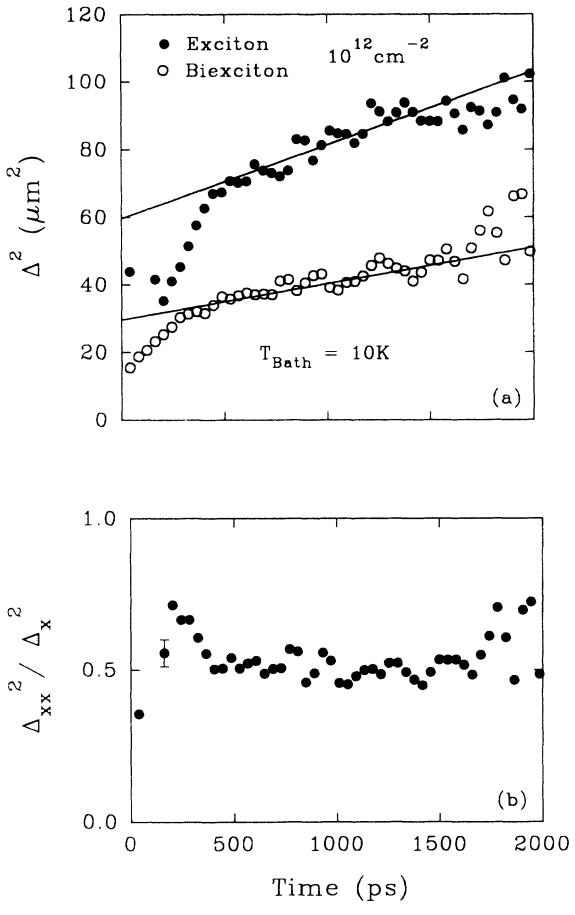

FIG. 8. (a) The squares of the spatial FWHM for the excitons and biexcitons are plotted as functions of time for an initial pair density of 10^{12} cm^{-2}. The instrumental FWHM has been deconvolved for the data points in this plot. (b) The ratio of the squares of the spatial FWHM cluster around 0.5, indicating that chemical equilibrium is maintained during the diffusive expansion. The error bar shows an estimate of the precision of our measurements.

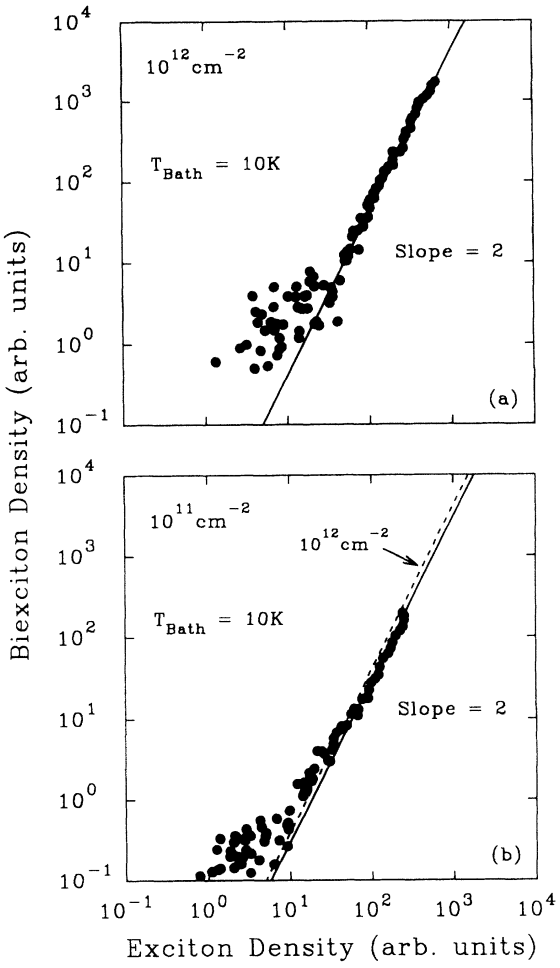

FIG. 9. (a) Exciton and biexciton densities plotted with time as the parametric variable for an initial pair density of 10^{12} cm^{-2} as in Fig. 5(b). Compared to Fig. 5(b), plotting the densities reveals an extended range over which the law of mass action describes the exciton-biexciton dynamics. (b) Exciton and biexciton densities plotted for an initial pair density of 10^{11} cm^{-2} which is 10% of the initial pair density in Fig. 9(a). Again, the law of mass action is valid over the density region where there is significant biexciton density. The square-law lines for the two initial densities nearly coincide with each other, as expected of a common equilibrium constant for a single equilibrium temperature.

V. DISCUSSION AND CONCLUSIONS

Although the observation of biexcitons is enhanced in GaAs MQW's compared to bulk GaAs, it had been generally believed that fast recombination would cause a deviation from the law of mass action. For example, Lovering and co-workers[7] found a subquadratic density dependence which they attributed to a competition between recombination and interconversion. Our time- and space-resolved experiments show, however, that a quadratic density dependence is quickly established and maintained over nearly three orders of magnitude in pair density, indicating that the excitons and biexcitons in our GaAs MQW exhibit a local chemical equilibrium. More-

over, the tight square-law dynamic behavior and self-consistent line shape for the biexciton add considerable strength over previous studies to the identification of the low-energy emission line with the biexcitonic molecule.

The data in Fig. 9 show a departure from the quadratic relationship at late times. There appear to be more biexcitons than predicted by the law of mass action. At such late times the biexciton strength is too small for accurate deconvolution, and it is possible that other species such as excitons bound to impurities contribute to the photoluminescence spectrum. Further work is required to resolve this issue.

The time-integrated data of Fig. 4 do not take into account the expanding area of the gas. The "apparent" gas area derived from the time-integrated spatial profile is not necessarily the appropriate area with which to normalize the intensity data. Since the interconversion occurring concurrently with the expansion affects the apparent area, there will be differences between the time-integrated measurements and a steady-state measurement. Indeed, normalizing the data of Fig. 4 by the time-integrated apparent area significantly reduces the exciton density at high excitation density and worsens the agreement with Eqs. (7).[14] Fortunately, time-resolved measurements avoid these problems.

The interesting rapid expansion observed before 500 ps has previously been observed by Yoon *et al.*[13] in a 210-Å GaAs MQW and also by Smith *et al.*[15] Yoon and coworkers showed that immediately following an intense 5-ps laser pulse in a 3-μm spot, the photoexcited carriers can expand laterally in the plane of the quantum well with diffusivity as high as 300 $cm^2 sec^{-1}$. Our data show that in the MQW used in this work, the initial rapid expansion also occurs with diffusivities of this magnitude. With increasing excitation density, the rapid expansion lasts longer, and the expansion coefficient increases. We postulate that the electron-hole plasma, observed at high excitation-densities,[16] may play an important role for the rapid expansion behavior which would also affect the thermodynamics of the excitons and biexcitons.

ACKNOWLEDGMENTS

This work was supported by the U.S. Department of Energy under Materials Research Laboratory Grant No. DEAC02-76ER01198. The experiments were performed in the Laser Laboratory Facility of the Frederick Seitz Materials Research Laboratory of the University of Illinois at Urbana-Champaign. We thank P. Bhattacharya of the Electrical Engineering Department and D. Steel of the Physics Department at the University of Michigan at Ann Arbor for the 100-Å GaAs MQW sample and for helpful discussions. We also thank M. Jiang for helpful comments.

[1]M. L. W. Thewalt and W. G. McMullan, Phys. Rev. B **30**, 6232 (1984); V. B. Timofeev, in *Excitons,* edited by E. I. Rashba and M. D. Sturge (North-Holland, Amsterdam, 1982), p. 349.

[2]P. L. Gourley and J. P. Wolfe, Phys. Rev. B **20**, 3319 (1979); **25**, 6338 (1983).

[3]R. L. Green, K. K. Bajaj, and D. E. Phelps, Phys. Rev. B **29**, 1807 (1984).

[4]D. A. Kleinman, Phys. Rev. B **28**, 871 (1982).

[5]R. C. Miller, D. A. Kleinman, A. C. Gossard, and O. Munteanu, Phys. Rev. B **25**, 6545 (1982).

[6]R. Cingolani, Y. Chen, and K. Ploog, Phys. Rev. B **38**, 13 478 (1988).

[7]D. J. Lovering, R. T. Phillips, G. J. Denton, and G. W. Smith, Phys. Rev. Lett. **23**, 1880 (1992); R. T. Phillips, D. J. Lovering, G. J. Denton, and G. W. Smith, Phys. Rev. B **45**, 4308 (1992).

[8]D. Oberhauser, K. H. Pantke, W. Langbein, V. G. Lyssenko, H. Kalt, J. M. Hvam, G. Weimann, and C. Klingshirn, Phys. Status Solidi B **173**, 53 (1992).

[9]A preliminary report was given in D. R. Wake, J. C. Kim, and J. P. Wolfe, *Quantum Electronics and Laser Science Conference,* Technical Digest Series Vol. 12 (Optical Society of America, Washington, D. C., 1993), p. 46.

[10]J. Feldmann, G. Peter. E. O. Göbel, P. Dawson, K. Moore, C. Foxon, and R. J. Elliot, Phys. Rev. Lett. **59**, 2337 (1987).

[11]H. Kume, K. Koyama, K. Nakatsugawa, S. Suzuki, and D. Fatlowitz, Appl. Opt. **27**, 1170 (1988).

[12]Kikuo Cho, Optics Commun. **8**, 412 (1973).

[13]H. W. Yoon, D. R. Wake, J. P. Wolfe, and H. Morkoç, Phys. Rev. B **46**, 13 461 (1992).

[14]For example, the initial excitation area is nearly equal to the initial exciton area for a generation rate below G_0 where the majority of the carriers are excitons. However, above G_0 the majority of the carriers exist as biexcitons instead. The initial excitation area is then approximately equal to the initial biexciton area and the equilibrium dynamics rapidly creates an exciton density profile whose diameter is 1.414 times larger. Our measurements show that the radiative emission rate is nearly constant over this density range, so that as the effective density increases as G is increased through G_0 the apparent areas measured in the time-integrated exciton and biexciton profiles increase by a factor of 1.414. Thus, unless far away from G_0 neither the exciton nor the biexciton area is a consistent measure of the area with which to normalize the intensities depicted in Fig. 4.

[15]L. M. Smith, J. S. Preston, J. P. Wolfe, D. R. Wake, J. Klem, T. Henderson, and H. Morokoç, Phys. Rev. B **39**, 1862 (1989).

[16]G. Tränkle, H. Leier, A. Forchel, H. Haug, C. Ell, and G. Weimann, Phys. Rev. Lett. **58**, 419 (1987).

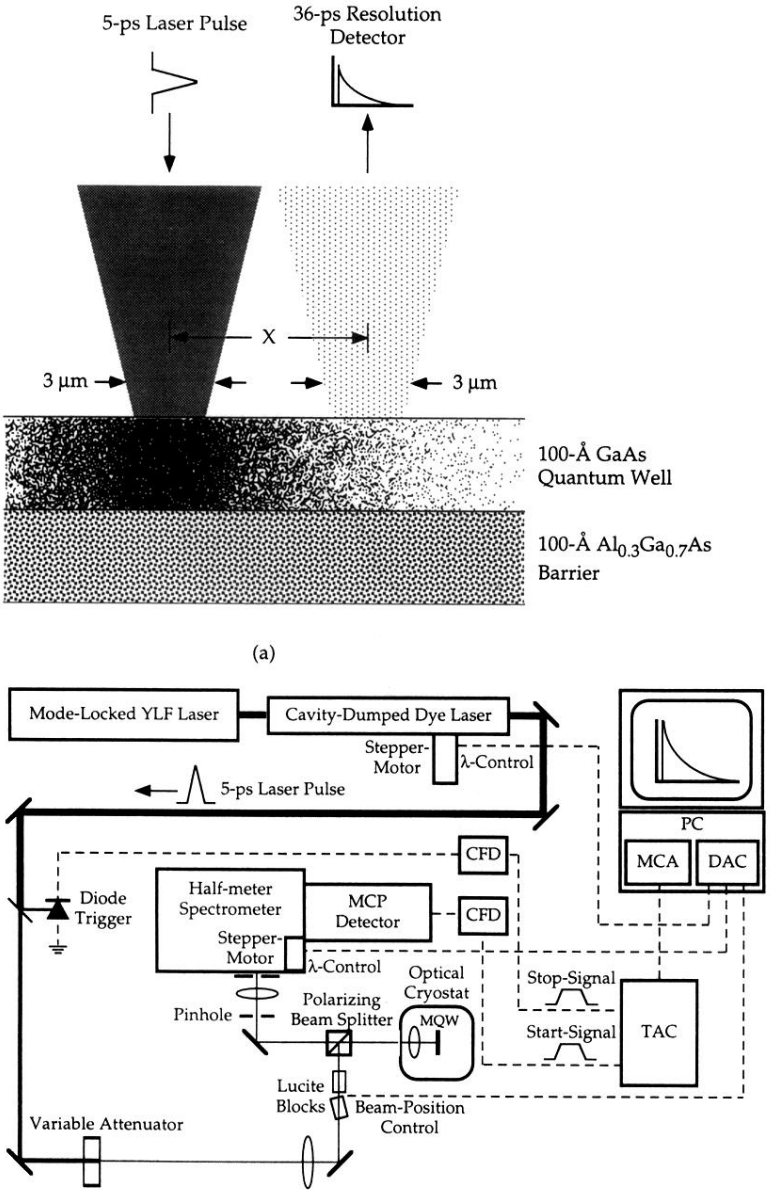

FIG. 2. (a) A schematic side view of the excitation area on the MQW sample. The detector field of view and the excitation spot can be moved (i.e., X changed in the figure) relative to each other for imaging. Inside the well, the strength of the shade indicates electron-hole pair density. (b) Time-correlated-photon-counting (TCPC) apparatus to measure time- and space-resolved photoluminescence. For more detail on the TCPC technique see Ref. 11.